# Resonance Raman Investigation of the MLCT Transition in $[Pt(dppm)_2(PhC{\equiv}C)_2]$ and the MMLCT Transition in $[Pt_2(\mu\text{-dppm})_2(\mu\text{-PhC}{\equiv}C)(PhC{\equiv}C)_2]^+$

**Wai Ming Kwok, David Lee Phillips,* Phyllis Kok-Yan Yeung, and Vivian Wing-Wah Yam***

*Department of Chemistry, University of Hong Kong, Pokfulam Road, Hong Kong*

*Received: July 29, 1997; In Final Form: September 26, 1997*[⊗]

We report resonance Raman spectra including absolute Raman cross section measurements obtained with excitation wavelengths within the MLCT absorption band of $[Pt(dppm)_2(PhC{\equiv}C)_2]$ and the MMLCT absorption band of $[Pt_2(\mu\text{-dppm})_2(\mu\text{-PhC}{\equiv}C)(PhC{\equiv}C)_2]^+$. We have simultaneously simulated the absolute absorption and resonance Raman intensities in order to estimate the vibrational reorganizational energies associated with the MLCT and MMLCT transitions. We observe a small amount of fluorescence background underneath the resonance Raman spectra of $[Pt(dppm)_2(PhC{\equiv}C)_2]$ which we attribute to emission from the very short-lived initially excited MLCT state. Our quantum yield measurements of this fluorescence yields an excited state lifetime of approximately 80−130 fs.

## Introduction

A great deal of work has been devoted to the study of the spectroscopic and photochemical properties of metal acetylides.[1−11] Photoexcitation of many of these metal acetylide molecular systems leads to photoluminescence and/or photochemical reactions with other compounds via a relatively long lived electronic excited state.[1−11] We have chosen to examine the initial photophysics of these compounds in order to characterize the initial electronic excited state at the vibrational mode specific level using resonance Raman spectroscopy. In particular, we want to investigate the photoinduced electron transfer reactions associated with the metal to ligand charge transfer (MLCT) transitions of platinum acetylide compounds. The results that we present here focus on $[Pt(dppm)_2(PhC{\equiv}C)_2]$ and $[Pt_2(\mu\text{-dppm})_2(\mu\text{-PhC}{\equiv}C)(PhC{\equiv}C)_2]^+$ in room temperature solutions.

The rates of electron transfer reactions are determined in part by the reorganization energies among the different vibrational modes of the molecules involved in the electron transfer.[12−18] The vibrational reorganizational energies in the case of electron-transfer reactions that take place directly upon absorption of light ($DA + h\nu \rightarrow D^+A^-$) can sometimes be obtained from the electron charge-transfer absorption and/or emission spectra.[19−28] Many charge-transfer absorption bands do not have vibrational resolution (especially in room temperature solutions), and in many cases it is not possible to elucidate the vibrational reorganizational energies directly from the absorption and/or fluorescence spectra. Several research groups have used resonance Raman intensity analysis in order to determine the vibrational reorganizational energies of many different photoinduced electron-transfer reactions which have diffuse charge transfer electronic transitions such as metal to ligand charge transfer (MLCT), ligand to ligand charge transfer (LLCT), intervalence transitions of inorganic compounds, organic noncovalent donor−acceptor complexes charge transfer transitions, and very recently an organic covalent donor−acceptor compound.[29−45]

In this paper we present a resonance Raman intensity analysis of the MLCT absorption at ∼344 nm for $[Pt(dppm)_2(PhC{\equiv}C)_2]$ in dichloromethane solution and of the MMLCT absorption band at ∼393 nm for $[Pt_2(\mu\text{-dppm})_2(\mu\text{-PhC}{\equiv}C)(PhC{\equiv}C)_2]^+$ in acetonitrile solution. We have taken resonance Raman spectra including absolute Raman cross section measurements at five excitation wavelengths for $[Pt(dppm)_2(PhC{\equiv}C)_2]$ and at six excitation wavelengths for $[Pt_2(\mu\text{-dppm})_2(\mu\text{-PhC}{\equiv}C)(PhC{\equiv}C)_2]^+$. The absolute Raman intensities and absorption spectra were simultaneously simulated using a simple model and time-dependent wavepacket calculations to find estimates of the vibrational reorganizational energies associated with the MLCT (metal to ligand charge transfer) and MMLCT (metal−metal to ligand charge transfer) transitions. We have also observed a weak broad fluorescence background underneath our resonance Raman spectra of $[Pt(dppm)_2(PhC{\equiv}C)_2]$ that we tentatively attribute to emission from the initially excited MLCT state of $[Pt(dppm)_2(PhC{\equiv}C)_2]$. Our quantum yield measurements of this fluorescence background are used to estimate the MLCT singlet excited state lifetime of ∼80−130 fs and this value is consistent with that found from modeling the absolute resonance Raman intensities and absorption spectrum. Finally, we discuss the implications of the ultrafast photophysics for the formation of the longer lived $^3$MLCT state of the platinum acetylides which leads to photoluminescence and/or photochemical reactions with other compounds.

## Experiment

Samples of $[Pt(dppm)_2(PhC{\equiv}C)_2]$ were synthesized using the literature method[46] and samples of the dinuclear A-frame complex $[Pt_2(\mu\text{-dppm})_2(\mu\text{-PhC}{\equiv}C)(PhC{\equiv}C)_2]ClO_4$ were synthesized by the reaction of phenylacetylene, mercury(II) acetate and $[Pt(dppm\text{-}P,P')_2]Cl_2$ in ethanol followed by metathesis reaction with lithium perchlorate as described previously.[6] The Raman experiments used sample solutions with concentrations of about $3.5 \times 10^{-3}$ M of $[Pt(dppm)_2(PhC{\equiv}C)_2]$ in dichloromethane solvent and $1.5 \times 10^{-3}$ M of $[Pt_2(\mu\text{-dppm})_2(\mu\text{-PhC}{\equiv}C)(PhC{\equiv}C)_2]ClO_4$ in acetonitrile solvent. The resonance Raman experimental apparatus and methods have been described previously.[47−52] Excitation frequencies for the resonance Raman experiments were generated by hydrogen Raman shifting the second, third, and fourth harmonics of a Spectra-Physics GCR-150-10 Nd:YAG laser. The flowing liquid jet sample or stirred cell sample was excited by a lightly focused laser beam (with

* Authors to whom correspondence should be addressed.

[⊗] Abstract published in *Advance ACS Abstracts,* November 15, 1997.

S1089-5639(97)02374-8 CCC: $14.00 

20−50 $\mu$J per pulse in ~1 mm diameter on the sample). An approximately 130° backscattering geometry was employed to collect the Raman scattered light with reflective optics (ellipsoidal mirror with *f*/1.4) to avoid chromatic aberrations from affecting the relative Raman intensities. This collected Raman scattered light passed through a depolarizer and the entrance slit of a 0.5 m spectrograph equipped with a 1200 groove/mm ruled grating blazed at 250 nm. The Raman scattered light was then dispersed onto a liquid nitrogen cooled CCD mounted on the exit port of the spectrograph. The Raman signal was collected from 60 to 120 s before being read out from the CCD to an interfaced PC clone computer and the resonance Raman spectrum was then obtained by summing up about 30−60 of these readout files.

Known frequencies of the dichloromethane or acetonitrile solvent Raman lines and several Hg lamp emission lines were used to calibrate the Raman shifts of the spectra, and appropriately scaled solvent spectra was subtracted to remove solvent lines. Any remaining reabsorption by the sample was corrected using previously described methods.[53] The spectra were intensity corrected for the detection system response (including any wavelength dependence of the ellipsoidal mirror, depolarizer, grating, mirrors of the monochromator, and the CCD response) by taking a spectrum of an intensity-calibrated tungsten lamp and comparison to its known lamp spectrum. Segments of the spectra were fit to a baseline plus a sum of Lorentzian peaks in order to obtain the integrated areas of the Raman peaks.

Absolute cross sections of the dichloromethane solvent were measured relative to previously reported absolute Raman cross sections of cyclohexane[54] in order to provide a reference for obtaining the absolute resonance Raman cross sections of $[Pt(dppm)_2(PhC{\equiv}C)_2]$. Previously published cross sections of acetonitrile[55] were used as a reference to find the absolute Raman cross sections of $[Pt_2(\mu\text{-dppm})_2(\mu\text{-PhC}{\equiv}C)(PhC{\equiv}C)_2]^+$. A Perkin Elmer Lambda 19 UV/vis spectrophotometer was used to spectrophotometrically obtain the concentrations of the $[Pt(dppm)_2(PhC{\equiv}C)_2]$/dichloromethane and of the $[Pt_2(\mu\text{-dppm})_2(\mu\text{-PhC}{\equiv}C)(PhC{\equiv}C)_2]^+$/acetonitrile samples before and after the Raman measurements. Variations of less than 5% during the experiment due primarily to evaporation of the solvent of the samples were observed for the measured absorption spectra used to find the concentrations for the absolute Raman cross section measurements. The absolute Raman cross sections were calculated from the average of a series of measurements and the depolarization ratio of the $[Pt(dppm)_2(PhC{\equiv}C)_2]$ and $[Pt_2(\mu\text{-dppm})_2(\mu\text{-PhC}{\equiv}C)(PhC{\equiv}C)_2]^+$ resonance Raman peaks were assumed to be 0.33. The maximum molar extinction coefficient of $[Pt(dppm)_2(PhC{\equiv}C)_2]$ in dichloromethane solution was experimentally determined to be 9290 $M^{-1}$ $cm^{-1}$. The experimental absolute Raman cross section at 354.7 nm for the 704 $cm^{-1}$ peak of dichloromethane was determined to be $4.76 \times 10^{-12}$ Å$^2$/molecule. The maximum molar extinction coefficient of $[Pt_2(\mu\text{-dppm})_2(\mu\text{-PhC}{\equiv}C)(PhC{\equiv}C)_2]^+$ in acetonitrile solution was experimentally determined to be 16 980 $M^{-1}$ $cm^{-1}$.

The integrated fluorescence intensity was found from the intensity-corrected combined resonance Raman and fluorescence spectrum. The fluorescence cross section was determined by comparing the integrated intensity of the fluorescence to the integrated intensity of the 2114 $cm^{-1}$ resonance Raman C≡C stretch peak and its determined absolute cross section. The fluorescence quantum yield is given by dividing the fluorescence cross section by the absorption cross section at the excitation wavelength.[56]

## Calculations

The calculations presented here are not intended to be a complete description of the photoinduced electron transfer process in the Franck−Condon region of the MLCT transition of **1** or the MMLCT transition of **2**. The simulations and model presented here are meant to provide a reasonable estimate of the vibrational reorganizational energies and short-time dynamics in the Franck−Condon region of the initially excited state as well as the contributions of inhomogeneous and homogeneous broadening processes to the absorption bandwidths of the MLCT transition of **1** and the MMLCT transition of **2**. The results presented here will also serve as a reference to which more sophisticated models and calculations can be compared to assess the importance of effects such as interference effects from smaller transitions nearby the dominant MLCT or MMLCT transition, changes in the transition dipole moment with vibrational coordinate, Duschinsky rotation of normal coordinates, vibrational dependent IC (internal conversion) rates, vibrational-dependent ISC (intersystem crossing) rates, IVR (intramolecular vibrational relaxation) rates on the initial excited state, and other effects on the resonance Raman, absorption, and fluorescence spectra.

The absorption spectrum and the resonance Raman intensities were simulated using a time-dependent formalism[57−66] and simple model. The absorption cross sections were calculated from the following expression:

$$\sigma_A(E_L) = (4\pi e^2 E_L M^2/3n\hbar^2 c) \int_{-\infty}^{\infty} d\delta\, G(\delta) \sum_i P_i \mathrm{Re}[\int_0^{\infty} \langle i|i(t)\rangle \exp[i(E_L-\epsilon_i)t/\hbar] \exp[-g(t)]\, dt] \quad (1)$$

The resonance Raman cross sections were calculated from this formula:

$$\sigma_R(E_L,\omega_s) = \int_{-\infty}^{\infty} d\delta\, G(\delta) \sum_i \sum_f P_i \sigma_{R,i\rightarrow f}(E_L)\, \delta(E_L + \epsilon_i - E_S - \epsilon_f)$$

with

$$\sigma_{R,i\rightarrow f}(E_L) = (8\pi e^4 {E_S}^3 E_L M^4/9\hbar^6 c^4) \left|\int_0^{\infty} \langle f|i(t)\rangle \exp[i(E_L+\epsilon_i)t/\hbar] \exp[-g(t)]\, dt\right|^2 \quad (2)$$

Equation 2 is generally applicable to a transition involving a single excited state. For our application to the dominant MLCT transition of **1** and MMLCT transition of **2** we have made a number of assumptions and these are detailed in the next few paragraphs. $M$ is the transition length (magnitude of transition dipole) evaluated at the equilibrium geometry, $n$ is the solvent index of refraction, $E_L$ is the incident photon energy, $E_S$ is the scattered photon energy, $P_i$ is the initial Boltzmann population of the ground-state vibrational level $|i\rangle$ which has energy $\epsilon_i$ (the number of initial vibrational energy levels included in the Boltzmann sum was up to $v = 2$ for the 180 $cm^{-1}$ mode), $\delta(E_L + \epsilon_i - E_S - \epsilon_f)$ is a delta function to add together cross sections with the same frequency, $|i(t)\rangle = e^{-iHt/\hbar}|i\rangle$ which is $|i(t)\rangle$ propagated on the excited state surface for a time $t$, $H$ is the excited state vibrational Hamiltonian, $f$ is the final state for the resonance Raman process, and $\epsilon_f$ is the energy of the ground-state vibrational level $|f\rangle$. The $\exp[-g(t)]$ term in eqs 1 and 2 is a damping function that depends on the nature of the electronic dephasing and in our system we chose to use an overdamped Brownian oscillator model.[67] The term $g(t)$ then has the following form

$$g(t) = (D/\Lambda)^2 (\Lambda t - 1 + \exp(-\Lambda t)) + i(D^2\Lambda/2kT)(1 - \exp(-\Lambda t)) + t/\tau \quad (3)$$

where the solvent is treated as a random perturbation that makes the solute energy levels fluctuate with a particular magnitude, $D$, and frequency, $\Lambda$. We assume that the temperature, $T$, is high enough that the frequencies of the solvent modes are very small relative to $kT$ and that all of the solvent modes are grouped together into one effective mode. The $t/\tau$ term represents the pure lifetime decay, and this term is found to be important for our present molecular systems.

The absorption cross sections and resonance Raman cross sections were calculated from eqs 1 and 2 by addition over a ground state Boltzmann distribution of vibrational energy levels. We have used harmonic oscillators with their potential minima offset by $\Delta$ in dimensionless normal coordinates (the displacements are defined with respect to the ground state frequency) to approximate the ground and excited state surfaces, and the harmonic oscillators could have either the same frequencies or different frequencies as appropriate. We also assumed no coordinate dependence of the transition length (Condon approximation). The time-dependent overlaps ($\langle i|i(t)\rangle$ and $\langle f|i(t)\rangle$) in eqs 1 and 2 were calculated numerically from analytic expressions of Mukamel and co-workers.[68] The vibrational reorganizational energies, $\lambda_v$, were found from the dimensionless normal coordinates ($\Delta$) using the following expressions:

$$\lambda_v = (\hbar\omega\Delta^2)/2 \quad \text{or} \quad \lambda_v = (\omega_e^2\Delta_g^2)/(2\omega_g) \quad (4)$$

where $\hbar\omega$ is the vibrational frequency of the Franck−Condon active vibrational modes.

## Results and Discussion

Figure 1 shows the geometry of $[Pt(dppm)_2(PhC{\equiv}C)_2]$ (**1**) and $[Pt_2(\mu\text{-dppm})_2(\mu\text{-PhC}{\equiv}C)(PhC{\equiv}C)_2]ClO_4$ (**2**) that are examined in this study. Figure 2 shows the absorption spectra of $[Pt(dppm)_2(PhC{\equiv}C)_2]$ in dichloromethane solvent and $[Pt_2(\mu\text{-dppm})_2(\mu\text{-PhC}{\equiv}C)(PhC{\equiv}C)_2]ClO_4$ in acetonitrile solvent with the excitation wavelengths for the resonance Raman experiments given as numbers in nm above the absorption spectra. The absorption band of $[Pt(dppm)_2(PhC{\equiv}C)_2]$ with a maximum at ca. 345 nm has been assigned to a predominantly metal to ligand charge transfer (MLCT) transition based on previously reported spectroscopic studies of $d^8$ metal acetylide complexes.[1,5−8] The absorption band of $[Pt_2(\mu\text{-dppm})_2(\mu\text{-PhC}{\equiv}C)(PhC{\equiv}C)_2]ClO_4$ with a maximum at ca. 393 nm has been attributed to a MMLCT transition.[6] The absorption bands of **1** and **2** were deconvoluted into a sum of Gaussians (dashed curves in Figure 2) so as to estimate the strength and position of the MLCT and MMLCT transitions. It would be quite helpful to have MCD spectra of these compounds to better estimate the transitions that compose the MLCT and MMLCT absorption bands, but no MCD spectra have been reported for these compounds to our knowledge. Figures 3 and 4 show an overview of the resonance Raman spectra of $[Pt(dppm)_2(PhC{\equiv}C)_2]$ and $[Pt_2(\mu\text{-dppm})_2(\mu\text{-PhC}{\equiv}C)(PhC{\equiv}C)_2]ClO_4$ which have been intensity corrected and solvent subtracted.

The resonance Raman spectra of **1** have many fundamental peaks as well as many overtone and combination band peaks. The peak positions and relative intensities of the 282.4, 319.9, 341.5, 354.7, and 368.9 nm resonance Raman spectra of **1** are given in Table 1. The relative intensity patterns for the four (368.9, 354.7, 341.5, and 319.9 nm) resonance Raman spectra of **1** obtained with excitation within the MLCT transition absorption ~345 nm are very similar to one another while the

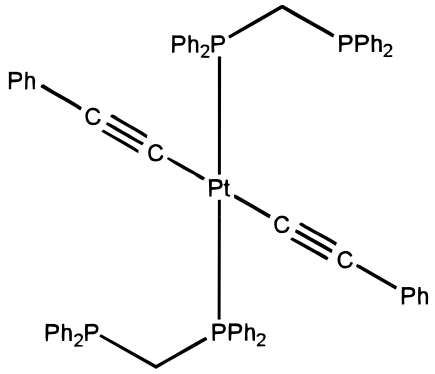


(1)

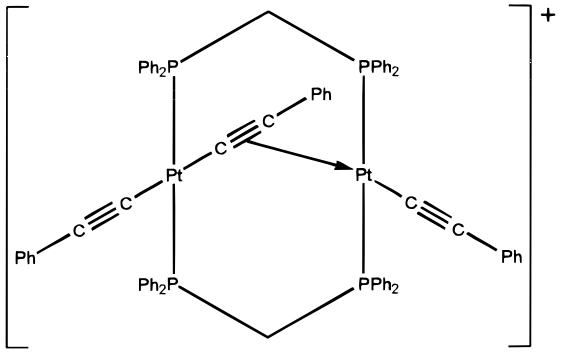


(2)

**Figure 1.** Geometry of $[Pt(dppm)_2(PhC{\equiv}C)_2]$ (**1**) and $[Pt(\mu\text{-dppm})_2(\mu\text{-PhC}{\equiv}C)(\mu\text{-PhC}{\equiv}C)_2]^+$ (**2**) examined in this study.

282.4 nm resonance Raman spectrum of **1** taken with excitation within the next higher energy absorption band displays a significantly different intensity pattern with many new Raman peaks (510, 532, and 2766 $cm^{-1}$) and much greater intensity in the 406, 428, 998, 1103, 1175, 1595, and 3190 $cm^{-1}$ Raman peaks. Table 1 also shows our absolute Raman cross section measurements for the large 2114 $cm^{-1}$ peak of **1**. The absolute cross section measurements follow the basic profile of the absorption spectra (see Figure 2). This and the very similar intensity patterns for the 354.7 and 341.5 nm resonance Raman spectra of **1** suggest that the resonance enhancement of these spectra are due mainly to the strong MLCT transition absorption band ca. 345 nm which accounts for 75−80% of the absorption coefficient at these wavelengths.

The resonance Raman spectra of **2** display almost all of their intensity in fundamental Raman peaks and we observed no appreciable Raman intensity above 2200 $cm^{-1}$ Raman shift. The monomer (**1**) resonance Raman spectra show only one very strong C≡C stretch peak ~2114 $cm^{-1}$ while the dimer (**2**) resonance Raman spectra have three very strong C≡C stretch peaks at 2027, 2062, and 2125 $cm^{-1}$ corresponding to the three different acetylide ligand environments. The dimer (**2**) strong C≡C stretch peaks are tentatively assigned as follows: the dimer terminal C≡C vibration that is trans to the $\sigma$-bonded $\mu$-PhC≡C$^-$ bridge to the 2125 $cm^{-1}$ peak in view of its close resemblance to the monomeric system, the $\mu$-bridging C≡C vibration to the lowest frequency wide 2027 $cm^{-1}$ peak, and the lone terminal C≡C vibration to the 2062 $cm^{-1}$ peak. Depending on the configuration of the dimer molecule and/or nearby solvent molecules at the time of photoexcitation it seems that the MMLCT electron transfer can go to any of the three acetylide acceptor ligands. Table 2 lists the relative Raman intensities

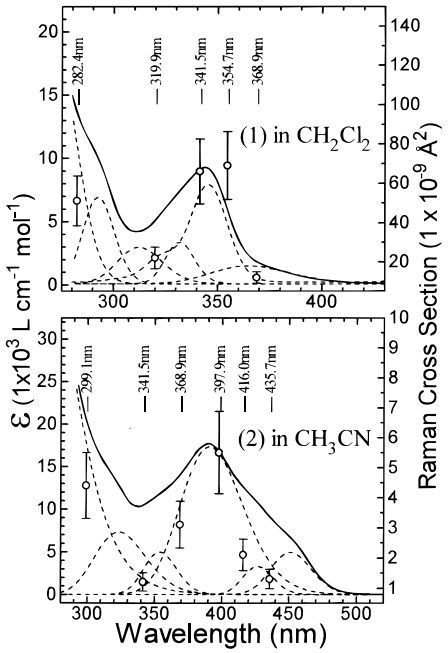


**Figure 2.** Absorption spectra of [Pt(dppm)$_2$(PhC≡C)$_2$] (**1**) in dichloromethane solution and [Pt($\mu$-dppm)$_2$($\mu$-PhC≡C)($\mu$-PhC≡C)$_2$]ClO$_4$ (**2**) in acetonitrile solution. The scale of the absorption spectra are indicated on the left axis. The excitation wavelengths for the resonance Raman experiments are given above each spectrum as numbers in nanometers. The dashed curves display a sum of Gaussian curves deconvolution of the absorption spectra. The experimental absolute Raman cross sections for the 2114 cm$^{-1}$ C≡C stretch of (**1**) and the 2125 cm$^{-1}$ C≡C stretch of (**2**) are also displayed as circles with error bars and the appropriate scale indicated on the right axis.

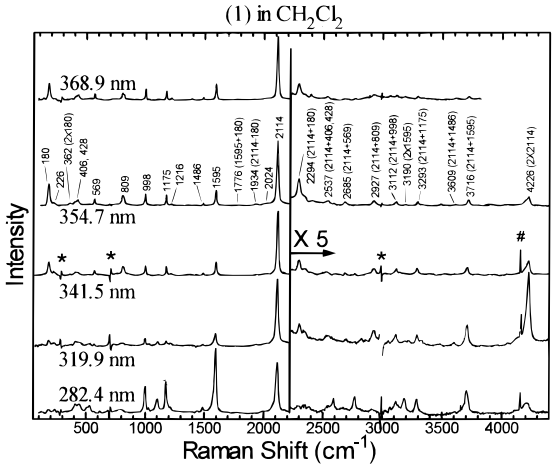


**Figure 3.** Overview of the resonance Raman spectra of [Pt(dppm)$_2$(PhC≡C)$_2$] (**1**) in dichloromethane solution. The spectra are intensity corrected, solvent subtracted, and background subtracted. Tentative assignments of some of the larger Raman peaks are also given. The asterisks mark regions where solvent subtraction artifacts are present and # represent ambient light or stray light features. A very large Raman-shifted laser line at 4155 cm$^{-1}$ in the 368.9 nm obscures the overtone of the 2114 cm$^{-1}$ mode and this part of the spectrum (3800−4300 cm$^{-1}$) is not shown in the 368.9 nm resonance Raman spectrum.

of **2** for excitation wavelengths of 299.1, 341.5, 368.9, 397.9, 416.0, and 435.7 nm. Table 2 also gives the absolute Raman cross sections for the 2125 cm$^{-1}$ peak of **2**. The absolute Raman cross sections for the 2125 cm$^{-1}$ peak and most of the others closely follow the absorption band profile and the 416.0, 397.9, and 368.9 nm spectra have similar intensity patterns for most of the Raman peaks. This could suggest that the 416.0, 397.9, and 368.9 nm resonance Raman spectra receive most of their resonance enhancement from the large MMLCT transition

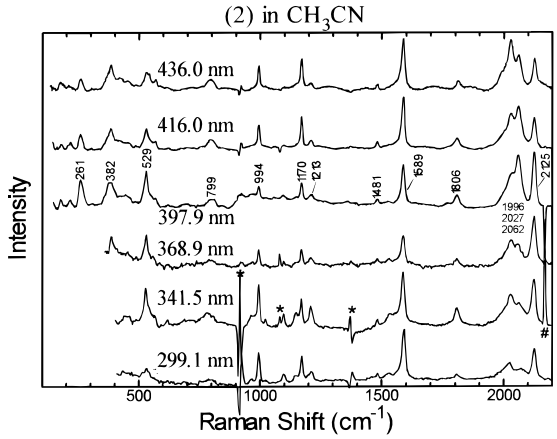


**Figure 4.** Overview of the resonance Raman spectra of [Pt($\mu$-dppm)$_2$($\mu$-PhC≡C)($\mu$-PhC≡C)$_2$]ClO$_4$ (**2**) in acetonitrile solution. The spectra are intensity corrected, solvent subtracted, and background subtracted. Tentative assignments of some of the larger Raman peaks are also given. The asterisks mark regions where solvent subtraction artifacts are present and # represent ambient light or stray light features. Part of the low-frequency region in the 299.1, 341.5, and 368.9 nm spectra are not shown since the Raman peaks are obscured by strong Rayleigh light scattering.

centered at 393 nm. However, we note that there is an interesting trend in the relative intensities of the three C≡C stretch peaks (2027, 2062, and 2125 cm$^{-1}$) in that the intensity of the 2125 cm$^{-1}$ peak is smallest on the red edge of the MMLCT absorption band and increases in intensity relative to the 2027 and 2062 cm$^{-1}$ peaks as one goes toward the blue edge of the MMLCT band. This could be an indication that there may be more than one configuration that contributes to the MMLCT absorption band. The different configurations may correspond to photoinduced electron transfer to different localized C≡C bonds. If the MMLCT state is degenerate, the depolarization ratios will be significantly different from the assumed 0.33 and the absolute cross sections measured will have noticeably different values. This would make a more complex analysis necessary to obtain accurate vibrational reorganizational energies. Thus, the analysis presented here for the MMLCT transition should be considered very preliminary and the values given as only an estimate in nature.

We have simultaneously simulated the absolute resonance Raman intensities and absorption spectra of **1** and **2** using time-dependent wavepacket calculations and the model described in the Calculations section in order to estimate the vibrational reorganizational energies for the initially excited MLCT or MMLCT state. For the initial MLCT state of **1** we focused on fitting the 341.5 and 354.7 nm Raman intensities (we placed approximately equal weight on the 341.5 and 354.7 nm Raman intensities) because the MLCT absorption extinction coefficients are stronger at these excitation wavelengths and it is much less likely that the smaller transitions on the red and blue edges of the absorption band will noticeably perturb the Raman intensities of the 341.5 and 354.7 nm Raman spectra. Similarly, we concentrated on the 397.9 nm resonance Raman intensities of **2** for simulating the initial MMLCT state. Tables 3 and 5 give the best fit parameters for modeling the resonance Raman intensities and absorption spectra of **1** and **2**. Figure 5 presents a comparison of the experimental, Gaussian deconvolution, and calculated MLCT and MMLCT absorption spectra of **1** and **2**, respectively. We obtain reasonably good agreement between the calculated and experimental Gaussian deconvolution estimate absorption spectra for both **1** and **2**. Tables 4 and 6 compare the experimental and calculated absolute Raman intensities using the parameters of Tables 3 and 5 and the simple model described

**TABLE 1: Resonance Raman Peaks of [Pt(dppm)$_2$(PhC≡C)$_2$] (1) in Dichloromethane Solution[a]**

| peak | Raman shift[b] (cm$^{-1}$) | intensity[c] 282.4 nm | 319.9 nm | 341.5 nm | 354.7 nm | 368.9 nm |
|---|---|---|---|---|---|---|
| F | 180 | 5.7 | 7.0 | 27.0 | 43.4 | 30.3 |
| F | 226 | 5.4 | 6.0 | 6.5 | 7.1 | |
| O (2 × 180) | 362 | | 1.1 | 1.8 | 4.1 | 4.8 |
| F | 406 | 14.5 | 5.6 | 5.9 | 7.3 | 7.2 |
| F | 428 | 21.8 | 12.7 | 4.4 | 7.2 | 12.8 |
| F | 510 | 8.6 | | | | |
| F | 532 | 8.2 | | | | |
| F | 569 | | 1.3 | 5.0 | 5.7 | 4.6 |
| F | 809 | 10.4 | 5.4 | 26.8 | 24.0 | 15.0 |
| F | 998 | 27.0 | 6.5 | 9.7 | 9.8 | 8.4 |
| F | 1103 | 25.6 | 5.0 | | | |
| F | 1175 | 28.4 | 6.2 | 8.6 | 8.8 | 7.5 |
| F | 1216 | 2.9 | 2.4 | 3.5 | 1.6 | 2.1 |
| F | 1486 | 4.8 | 1.1 | 1.8 | 1.3 | 1.5 |
| F | 1595 | 99.5 | 21.0 | 18.3 | 18.3 | 20.1 |
| C (1595 + 180) | 1776 | | | 0.6 | 2.3 | 0.7 |
| F | 1902 | | | | 2.7 | |
| C (2114 − 180) | 1934 | | 1.8 | 2.1 | 2.6 | 1.2 |
| F | 1995 | 3.5 | | 4.6 | 1.2 | 0.9 |
| F | 2024 | | 2.7 | 1.8 | 4.2 | 3.3 |
| F | 2114 | 100.0 | 100.0 | 100.0 | 100.0 | 100.0 |
| absol Raman cs of 2114 (Å$^2$/molecule) | | [5.1 × 10$^{-8}$] | [2.2 × 10$^{-8}$] | [6.6 × 10$^{-8}$] | [6.9 × 10$^{-8}$] | [1.2 × 10$^{-8}$] |
| | 2177 | 4.4 | | | | |
| C (2114 + 180) | 2294 | | 4.3 | 5.4 | 13.5 | 7.0 |
| C (2114 + 226) | 2339 | | 2.7 | 2.0 | 1.9 | 1.3 |
| C (2114 + 406, 428) | 2537 | 12.5 | 7.4 | 3.9 | 2.7 | 1.6 |
| C (2114 + 569) | 2685 | | 0.9 | 0.5 | 1.7 | 0.4 |
| C (1595 + 1175) | 2766 | 5.6 | | | | |
| C (2114 + 809) | 2927 | | 9.8 | 4.1 | 2.1 | 3.5 |
| C (2114 + 998) | 3112 | 7.8 | 4.1 | 3.7 | 1.6 | 0.8 |
| O (2 × 1595) | 3190 | 6.2 | 2.3 | | 0.3 | |
| C (2114 + 1103) | 3211 | | 4.9 | | | |
| C (2114 + 1175) | 3293 | 6.2 | 3.1 | 2.9 | 1.4 | 0.7 |
| C (2114 + 1215) | 3329 | | 2.4 | | | |
| C (2114 + 1486) | 3609 | | | | 0.4 | 0.6 |
| C (2114 + 1595) | 3716 | 13.5 | 8.8 | 3.7 | 2.5 | 1.1 |
| O (2 × 2114) | 4226 | 10.9 | 37.0 | 11.4 | 4.8 | |

[a] F = fundamental, O = overtone, and C = combination band; c.s. = cross section. [b] Estimated uncertainties are about 4 cm$^{-1}$ for the Raman shifts. [c] Relative intensities are based on integrated areas of the peaks. Estimated uncertainties are about 5% for intensities 30 and higher, 10% for intensities between 5 and 30, and 20% for intensities lower than 5.

in the Calculations section. We find reasonable agreement between our calculated and experimental resonance Raman intensities and absolute Raman cross sections of **1** for 341.5 and 354.7 nm. There are noticeably greater differences between the calculated and experimental resonance Raman intensities and absolute Raman cross sections of **1** for the 319.9 and 368.9 nm excitation wavelengths and this is most likely due to the larger contributions of other transitions to the absorption coefficients at these wavelengths. We also find reasonable agreement between our experimental and calculated absolute Raman intensities for **2** at 397.9 nm near the center of the MMLCT absorption band where the MMLCT transition has the dominant contribution to the absorption band. We do not see very good agreement for **2** near the blue (368.9 nm) or red edges (416.0 and 435.7 nm) of the MMLCT absorption presumably due to other transitions making more significant contributions to the resonance Raman intensities.

We needed to use a large amount of inhomogeneous broadening (690 cm$^{-1}$ standard deviation) and a moderate amount of homogeneous broadening (200 cm$^{-1}$ fwhm plus a 45 cm$^{-1}$ hwhm population decay) to fit the absorption spectra and absolute Raman cross sections of **1**. Investigations on similar compounds like Pt(C≡CH)$_2$(PEt$_3$)$_2$ in 77 K glasses exhibited strong emission heterogeneity attributed to site heterogeneity[1] and this is consistent with the observation that our simulations of the absorption spectra and absolute Raman cross sections needed a large amount of inhomogeneous broadening to model adequately. It is interesting to note that a resonance Raman intensity analysis on a covalent dicyanoethylene−azaadamantane[45] charge transfer band ∼300 nm in the solution phase found both large "inhomogeneous" (standard deviation of 2000 cm$^{-1}$) and "homogeneous" (1500 cm$^{-1}$ fwhm) contributions to the absorption bandwidth. It would be very useful to have other experimental studies such as hole-burning experiments done on **1** or similar inorganic complexes in order to better characterize and independently corroborate the inhomogeneous broadening indicated by our resonance Raman analysis of **1**.

The noticeable amounts of homogeneous broadening needed in our calculations indicate that there is a significant degree of population decay and/or electronic dephasing for the initial excited states of **1** and **2**. Electronic dephasing of these fairly large molecules in room temperature solutions would be expected to be fairly large with the dephasing rate faster for **2** than **1** which is consistent with our homogeneous broadening parameters for **2** ($\Gamma$ = 2500 cm$^{-1}$ fwhm) and **1** ($\Gamma$ = 200 cm$^{-1}$ fwhm). The small amount of fluorescence observed for both **1** and **2** suggests that the population decay probably makes significant contributions to the total homogeneous broadening.

Tables 3 and 5 also list the vibrational reorganizational energies associated with the initial MLCT state of **1** and the

**TABLE 2: Resonance Raman Peaks of $[Pt_2(\mu\text{-dppm})_2(\mu\text{-PhC}{\equiv}C)(PhC{\equiv}C)_2]ClO_4$ (2) in Acetonitrile Solution[a]**

| peak | Raman shift[b] ($cm^{-1}$) | intensity[c] 299.1 nm | 341.5 nm | 368.9 nm | 397.9 nm | 416.0 | 435.7 nm |
|---|---|---|---|---|---|---|---|
| F | 179 | *d* | | *d* | 17 | 8 | 22 |
| F | 216 | *d* | | *d* | 19 | 14 | 12 |
| F | 261 | *d* | | *d* | 100 | 39 | 26 |
| F | 382 | *d* | | *d* | 140 | 85 | 87 |
| F | 421 | *d* | | *d* | 26 | 23 | 20 |
| F | 452 | 36 | 42 | *d* | 62 | 27 | 38 |
| F | 529 | 44 | 66 | 97 | 103 | 55 | 44 |
| F | 552 | | 28 | 24 | 23 | 17 | 6 |
| F | 568 | | | | 18 | 7 | 23 |
| F | 799 | 37 | 86 | 36 | 61 | 45 | 49 |
| F | 967 | 5 | 16 | 20 | 14 | | |
| F | 994 | 43 | 35 | 36 | 21 | 33 | 27 |
| F | 1095 | 14 | 15 | 7 | 11 | | |
| F | 1147 | 9 | 29 | 13 | 5 | | |
| F | 1170 | 35 | 31 | 37 | 30 | 42 | 42 |
| F | 1213 | 24 | 40 | 39 | 21 | 15 | 10 |
| F | 1481 | 5 | 6 | 8 | 7 | 7 | 6 |
| F | 1529 | 8 | 30 | 8 | 5 | | |
| F | 1589 | 100 | 100 | 100 | 100 | 100 | 100 |
| absol Raman c.s. of 1589 $cm^{-1}$ peak ($Å^2$/molecule) | | $[6.8 \times 10^{-9}]$ | $[1.2 \times 10^{-9}]$ | $[1.5 \times 10^{-9}]$ | $[3.6 \times 10^{-9}]$ | $[3.3 \times 10^{-9}]$ | $[1.9 \times 10^{-9}]$ |
| C (1589 + 179) | 1766 | | | | 13 | | |
| F | 1806 | 12 | 52 | 44 | 45 | 41 | 16 |
| F | 1996 | 51 | 67 | 56 | 53 | 65 | 75 |
| F | 2027 | 40 | 82 | 124 | 167 | 111 | 153 |
| F | 2062 | 50 | 109 | 116 | 217 | 140 | 81 |
| F | 2125 | 65 | 101 | 205 | 151 | 64 | 68 |
| absol Raman c.s. of 2125 $cm^{-1}$ peak ($Å^2$/molecule) | | $[4.4 \times 10^{-9}]$ | $[1.2 \times 10^{-9}]$ | $[3.1 \times 10^{-9}]$ | $[5.5 \times 10^{-9}]$ | $[2.1 \times 10^{-9}]$ | $[1.3 \times 10^{-9}]$ |

[a] F = fundamental, O = overtone, and C = combination band; c.s. = cross section. [d] Low-frequency region obscured in the 299.1, 341.5, and 368.9 nm spectra due to strong scattered Rayleigh light. [b] Estimated uncertainties are about 4 $cm^{-1}$ for the Raman shifts. [c] Relative intensities are based on integrated areas of the peaks. Estimated uncertainties are about 10% for intensities 50 and higher, 15% for intensities between 15 and 50, and 30% for intensities lower than 15.

**TABLE 3: Parameters for Simulations of Resonance Raman Intensities and Vibrational Reorganizational Energies of $[Pt(dppm)_2(PhC{\equiv}C)_2]$ (1) in Dichloromethane Solution[a]**

| ground state vibrnl freq ($cm^{-1}$) | excited state freq ($cm^{-1}$) | $\|\Delta\|$ | vibrnl reorganizational energy ($cm^{-1}$) |
|---|---|---|---|
| 180 | 180 | 0.382 | 13 |
| 226 | 226 | 0.197 | 4 |
| 406 | 406 | 0.122 | 3 |
| 428 | 428 | 0.129 | 3.6 |
| 569 | 569 | 0.115 | 4 |
| 809 | 809 | 0.206 | 17 |
| 998 | 998 | 0.175 | 15 |
| 1175 | 1175 | 0.171 | 17 |
| 1216 | 1216 | 0.084 | 4 |
| 1486 | 1486 | 0.075 | 4 |
| 1595 | 1595 | 0.255 | 52 |
| 1995 | 1995 | 0.101 | 10 |
| 2024 | 2024 | 0.101 | 10 |
| 2114 | 2114 | 0.620 | 406 |
| | | | total $\lambda_v = 562.6$ |

transition length, $M = 0.61$ Å, $E_0 = 28\,860$ $cm^{-1}$, $n = 1.45$
lifetime broadening, $\Gamma = 45$ $cm^{-1}$ hwhm
homogeneous broadening, $\Gamma = 200$ $cm^{-1}$ fwhm
inhomogeneous broadening, $G = 690$ $cm^{-1}$ standard deviation
Brownian oscillator $\Lambda/D = 0.1$, $\Lambda = 8.64$ $cm^{-1}$, $D = 86.43$ $cm^{-1}$

[a] Calculated using the parameters of this table in eqs 1−4 and the model described in the Calculations section.

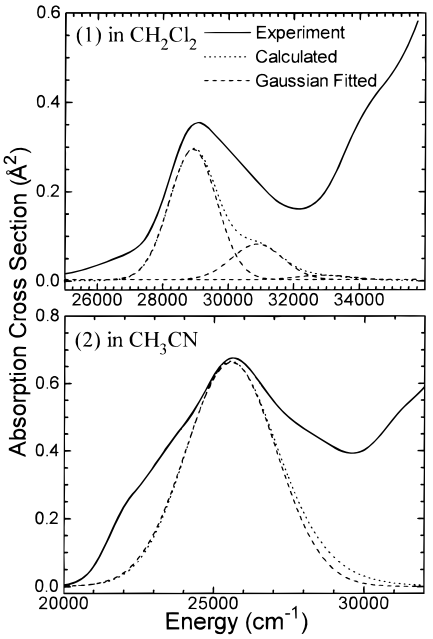


**Figure 5.** Comparison of experimental (solid lines) with calculated (dotted lines) absorption spectra of **1** and **2**. The Gaussian curves (dashed lines) found from deconvolution of the experimental absorption spectra which estimate the strength and positions of the MLCT and MMLCT transitions of **1** and **2**, respectively, are also shown.

MMLCT state of **2**. The internal reorganizational energies are partitioned among many different vibrational modes with a wide range of vibrational frequencies. We note that the total internal reorganizational energies for **1** and **2** are noticeably smaller than those reported for MLCT transitions of other inorganic complexes. About 70% of the internal reorganizational energy of **1** appears in the nominal C≡C stretch mode at 2114 $cm^{-1}$ which is associated with the acetylide ligands. Only a fairly small amount of internal reorganizational energy shows up in the low-frequency vibrational modes below 1000 $cm^{-1}$ that may be associated with the metal portion of **1**. The 180 $cm^{-1}$ mode of **1** is likely due to the $\delta$(P−Pt−P) bending mode.[69] In general, the vibrational reorganizational energies we find for **1** are consistent with changes in the structure of both the metal and

**TABLE 4: Comparison of Experimental and Calculated Resonance Raman Intensities of [Pt(dppm)$_2$(PhC≡C)$_2$] (1) in Dichloromethane Solution[a]**

| | | intensity | | | | | | | |
|---|---|---|---|---|---|---|---|---|---|
| | Raman | 319.9 nm | | 341.5 nm | | 354.7 nm | | 368.9 nm | |
| peak | shift[b] (cm$^{-1}$) | expt[c] | calc | expt[c] | calc | expt[c] | calc | expt[c] | calc |
| F | 180 | 7.0 | 3.3 | 27.0 | 47.1 | 43.4 | 45.1 | 30.3 | 30.8 |
| F | 226 | 6.0 | 0.9 | 6.5 | 13.1 | 7.1 | 12 | | 7.9 |
| O (2 × 180) | 362 | 1.1 | 0.3 | 1.8 | 4.4 | 4.1 | 3.4 | 4.8 | 1.9 |
| F | 406 | 5.6 | 0.8 | 5.9 | 10.3 | 7.3 | 7.9 | 7.2 | 4.8 |
| F | 428 | 12.7 | 0.7 | 4.4 | 9.1 | 7.2 | 6.9 | 12.8 | 4.3 |
| F | 569 | 1.3 | 0.6 | 5.0 | 7.7 | 5.7 | 5.3 | 4.6 | 3.4 |
| F | 809 | 5.4 | 2.9 | 26.8 | 23.3 | 24.0 | 15.0 | 15.0 | 10.8 |
| F | 998 | 6.5 | 2.8 | 9.7 | 15.3 | 9.8 | 9.9 | 8.4 | 7.8 |
| F | 1175 | 6.2 | 3.6 | 8.6 | 13.2 | 8.8 | 8.9 | 7.5 | 7.5 |
| F | 1216 | 2.4 | 0.9 | 3.5 | 3.1 | 1.6 | 2.1 | 2.1 | 1.8 |
| F | 1486 | 1.1 | 1.2 | 1.8 | 2.1 | 1.3 | 1.6 | 1.5 | 1.5 |
| F | 1595 | 21.0 | 15.4 | 18.3 | 22.1 | 18.3 | 18.1 | 20.1 | 16.9 |
| C (1595 + 180) | 1776 | | 1.5 | 0.6 | 1.6 | 2.3 | 1.2 | 0.7 | 0.8 |
| C (2114 − 180) | 1934 | 1.8 | 1.8 | 2.1 | 1.7 | 2.6 | 2.2 | 1.2 | 2.2 |
| F | 1995 | | 2.7 | 4.6 | 2.8 | 1.2 | 2.7 | 0.9 | 2.7 |
| F | 2024 | 2.7 | 2.7 | 1.8 | 2.8 | 4.2 | 2.7 | 3.3 | 2.7 |
| F | 2114 | 100.0 | 100.0 | 100.0 | 100.0 | 100.0 | 100.0 | 100.0 | 100.0 |
| expt absol Raman c.s. of 2114 (Å$^2$/molecule) | | [2.2 × 10$^{-8}$] | | [6.6 × 10$^{-8}$] | | [6.9 × 10$^{-8}$] | | [1.2 × 10$^{-8}$] | |
| calc absol Raman c.s. of 2114 (Å$^2$/molecule) | | (7.3 × 10$^{-8}$) | | (8.6 × 10$^{-8}$) | | (4.6 × 10$^{-8}$) | | (3.4 × 10$^{-9}$) | |
| C (2114 + 180) | 2294 | 4.3 | 7.9 | 5.4 | 7.4 | 13.5 | 6.9 | 7.0 | 4.6 |
| C (2114 + 226) | 2339 | 2.7 | 2.2 | 2.0 | 2.1 | 1.9 | 1.8 | 1.3 | 1.2 |
| C (2114 + 406, 428) | 2537 | 7.4 | 3.2 | 3.9 | 3.0 | 2.7 | 2.3 | 1.6 | 1.3 |
| C (2114 + 569) | 2685 | 0.9 | 1.3 | 0.5 | 1.2 | 1.7 | 0.8 | 0.4 | 0.5 |
| C (2114 + 809) | 2927 | 9.8 | 3.9 | 4.1 | 3.7 | 2.1 | 2.3 | 3.5 | 1.5 |
| C (2114 + 998) | 3112 | 4.1 | 2.7 | 3.7 | 2.4 | 1.6 | 1.5 | 0.8 | 1.1 |
| O (2 × 1595) | 3190 | 2.3 | 1.1 | | 0.5 | 0.3 | 0.3 | | 0.2 |
| C (2114 + 1175) | 3293 | 3.1 | 2.5 | 2.9 | 2.1 | 1.4 | 1.3 | 0.7 | 1.0 |
| C (2114 + 1215) | 3329 | 2.4 | 0.6 | | 0.5 | | 0.3 | | 0.2 |
| C (2114 + 1486) | 3609 | | 0.5 | | 0.3 | 0.4 | 0.2 | 0.6 | 0.2 |
| C (2114 + 1595) | 3716 | 8.8 | 6.0 | 3.7 | 3.7 | 2.5 | 2.7 | 1.1 | 2.3 |
| O (2 × 2114) | 4226 | 37.0 | 38.2 | 11.4 | 9.2 | 4.8 | 7.4 | | 6.5 |

[a] F = fundamental, O = overtone, and C = combination band; c.s. = cross section. The fit of the simulations only focused on the 341.5 and 354.7 nm data which were given about equal weight (see text). [b] Estimated uncertainties are about 4 cm$^{-1}$ for the Raman shifts. [c] Experimental relative intensities are based on integrated areas of the peaks. Estimated uncertainties are about 5% for intensities 30 and higher, 10% for intensities between 5 and 30, and 20% for intensities lower than 5.

ligand parts of the molecule that one would expect to find for a MLCT transition.

Figure 6 displays the 319.9, 341.5, and 354.7 nm resonance Raman spectra of **1** (these spectra have been intensity corrected and solvent subtracted) with the background signal underneath the resonance Raman peaks. The background signal in Figure 6 has been deconvoluted into a portion that is due to scattered laser light (not shown) and a Gaussian portion (dashed line) that is tentatively assigned to fluorescence from the excited MLCT state of **1**. We estimated the rate constant for radiative decay from the Einstein coefficient for spontaneous emission:

$$k_R = (64\pi^4 e^2 \nu_{mm}{}^3 M_{mm}{}^2)/3h \qquad (5)$$

where $\nu_{mm}$ is the electronic transition frequency and $M_{mm}$ is the transition length. Using an absorption maximum of 29 090 cm$^{-1}$ and a transition length of 0.61 Å (obtained from the fit to the dominant MLCT transition ~340 nm) we obtain $k_R = 6.0 \times 10^7$ s$^{-1}$. The integrated fluorescence cross section at 354.7 nm was found to be ~$1.44 \times 10^{-6}$ Å$^2$/molecule and the absorption cross section at 354.7 nm was 0.176 Å$^2$/molecule (for 341.5 nm the values are ~$1.69 \times 10^{-6}$ Å$^2$/molecule and 0.292 Å$^2$/molecule, respectively). This gives an estimated fluorescence quantum yield ($\Phi_F$) of ~$8.2 \times 10^{-6}$ for 354.7 nm and $\Phi_f$ ~$5.8 \times 10^{-6}$ for 341.5 nm. Using the fluorescence quantum yield and the radiative rate constant we estimate the excited state lifetime to be ~136 fs at 354.7 nm and ~86 fs at 341.5 nm. The nonradiative rate constant ($k_{NR}$) can be found from

$$k_{NR} = (k_R/\Phi_F) - k_R \qquad (6)$$

and this gives $k_{NR} = 7.3 \times 10^{12}$ s$^{-1}$ at 354.7 nm and $k_{NR} = 1.2 \times 10^{13}$ s$^{-1}$ at 341.5 nm for the MLCT excited state of **1**. Thus, nonradiative processes are the dominant population decay mechanism of the MLCT excited state for **1**. The phenomenological homogeneous line width that best fit the resonance Raman cross sections of **1** has three possible significant contributions: excited state population decay, dynamics along modes not modeled in the calculation, and solvent dephasing. The contribution from excited state population decay is large (~45 cm$^{-1}$ hwhm from the fit given in Table 3) but does not account for all of the homogeneous line width we needed to fit the absolute Raman cross sections and this suggests that solvent dephasing also makes a noticeable contribution to the total homogeneous linewidth. Inspection of the fluorescence for the initial MLCT excited state of **1** shown in Figure 6 reveals that the fluorescence band shape is quite asymmetric and blue-shifted. This suggests that the fluorescence is mainly from vibrationally unrelaxed excited states and that the fluorescence and nonradiative transfer mechanisms proceed mostly from a nonequilibrated excited MLCT state. Our resonance Raman intensity analysis homogeneous broadening parameters and our fluorescence quantum yield measurements indicate that both

**TABLE 5: Parameters for Simulations of Resonance Raman Intensities and Vibrational Reorganizational Energies of $[Pt_2(\mu\text{-dppm})_2(\mu\text{-PhC}{\equiv}C)(PhC{\equiv}C)_2]ClO_4$ (2) in Acetonitrile Solution**

| ground state vibrnl freq ($cm^{-1}$) | excited state freq ($cm^{-1}$) | $\|\Delta\|$ | vibrnl reorganizational energy ($cm^{-1}$) |
|---|---|---|---|
| 179 | 179 | 0.4431 | 18 |
| 216 | 216 | 0.4408 | 21 |
| 261 | 261 | 0.846 | 93 |
| 382 | 382 | 0.6941 | 92 |
| 421 | 421 | 0.2738 | 16 |
| 452 | 452 | 0.3946 | 35 |
| 529 | 529 | 0.4406 | 51 |
| 552 | 552 | 0.2002 | 11 |
| 568 | 568 | 0.1727 | 8 |
| 799 | 799 | 0.236 | 22 |
| 967 | 967 | 0.0969 | 4 |
| 994 | 994 | 0.116 | 7 |
| 1095 | 1095 | 0.0783 | 3 |
| 1147 | 1147 | 0.0505 | 1 |
| 1170 | 1170 | 0.1231 | 9 |
| 1213 | 1213 | 0.1005 | 6 |
| 1481 | 1481 | 0.0509 | 2 |
| 1529 | 1529 | 0.0421 | 1 |
| 1589 | 1589 | 0.1863 | 28 |
| 1806 | 1806 | 0.1181 | 13 |
| 1996 | 1996 | 0.1234 | 15 |
| 2027 | 2027 | 0.2188 | 48 |
| 2062 | 2062 | 0.248 | 63 |
| 2125 | 2125 | 0.2051 | 45 |
| | | | total $\lambda_v = 612$ |

transition length, $M$ 1.20 Å, $E_0 = 22\,300$ $cm^{-1}$, $n = 1.344$
lifetime broadening, $\Gamma = 50$ $cm^{-1}$ hwhm
homogeneous broadening, $\Gamma = 2500$ $cm^{-1}$ fwhm
inhomogeneous broadening, $G = 850$ $cm^{-1}$ standard deviation
Brownian oscillator $\Lambda/D = 0.01$, $\Lambda = 10.6$ $cm^{-1}$, $D = 1060$ $cm^{-1}$

[a] Calculated using the parameters of this table in eqs 1−4 and the model described in the Calculations section.

population decay and electronic dephasing are occurring on similar time scales. This is also consistent with the fluorescence of the initial excited MLCT state being due to emission from a nonequilibrated excited state. The effect of the excited state lifetime on the absorption, resonance Raman, and fluorescence spectra has been explored with a single solute mode with a single Brownian oscillator solvent mode model.[67] These calculations showed that as the excited state lifetime becomes very small and is comparable to the solvent relaxation time, the fluorescence quantum yield becomes very small and the fluorescence band shape becomes significantly blue-shifted, indicating that there is not enough time for the fluorescence to proceed to its full Stokes shift.[67] In other words, the fluorescence is mainly due to emission from an unequilibrated (unrelaxed) excited state. These model calculations are consistent with our interpretation of the fluorescence of the initial excited MLCT state as being due to emission from an unequilibrated excited state. There have been many other experimental measurements of unrelaxed fluorescence, including observation of "lifetime" gating of the Stokes shift in steady-state experiments[70] and time-dependent Stokes shifts in ultrafast time-resolved fluorescence experiments.[71]

The excited state lifetime of the initial excited MLCT state of **1** likely has important implications for both the observed internal reorganizational energy and the photochemistry associated with the photoinduced electron transfer associated with MLCT transitions in Pt acetylide complexes (and possibly many other inorganic systems). Many models of excited state relaxation usually assume that IVR is much faster than IC which is much faster than ISC with the rate constants ordered as follows: $k_{IVR} \gg k_{IC} \gg k_{ISC}$. This type of model leads to a relaxation from the initial Franck−Condon part of the excited potential energy surface of that electronic state to the lowest energy of that state before moving on to the next electronic state via IC or ISC. Our results provide experimental evidence (both absolute resonance Raman cross sections and intensities as well as fluorescence quantum yields and fluorescence band shape) that indicates that these general models of excited state relaxation are inadequate for MLCT transitions of **1** and possibly other similar inorganic compounds in which the excited-state lifetime competes effectively with IVR so that IC and/or ISC occur mostly from unrelaxed and/or partially relaxed states in or near the Franck−Condon region of the initial excited state. Inspection of the vibrational reorganizational energies shows most (∼70%) of the internal reorganizational of **1** appears in the nominal C≡C stretch mode. Most of the motion of the initial MLCT excited state would also be along this mode. Emissions from the $^3$MLCT states of related platinum complexes, $[Pt(C{\equiv}CPh)_2(PEt_3)_2]$ and $[Pt(C{\equiv}CH)_2(PEt_3)_2]$, exhibit very strong vibrational progressions in the C≡C stretch ligand mode, indicating that there is a large distortion of this mode in the $^3$MLCT states.[1] This and our current results strongly suggest that initial excitation of the $^1$MLCT state leads to mostly motion along the C≡C stretch mode to a region of strong overlap with the $^3$MLCT resulting in ISC at a very fast rate that competes effectively with IC and IVR on the $^1$MLCT state. Our simulations of the absolute resonance Raman intensities of the MLCT transition of **1** using a Brownian oscillator model for the solvent indicate that solvent relaxation is occurring on a similar time scale (within a factor of 10) as the excited state decays via ISC and/or IC.

We note that very recent and elegant femtosecond time-resolved transient absorption experiments on the $[Ru(bpy)_3]^{2+}$ system by McCusker and co-workers[72] followed the formation of the $^1$MLCT excited state and subsequent formation of the $^3$MLCT excited state and found that the decay of the $^1$MLCT state and formation of the $^3$MLCT state was complete in 300 fs with a half-life of 100 fs. Their transient absorption spectra of the $^1$MLCT state of $[Ru(bpy)_3]^{2+}$ displayed complex evolution with time, indicating that dynamical processes were taking place in the $^1$MLCT state as it decayed. They noted that their $CH_3CN$ solvent has inertial solvent response times in the 100 fs range[73−76] and that the $^1$MLCT excited state would have a large dipole moment suggesting that solvent relaxation is concurrent with the $^1$MLCT dynamics. McCusker and co-workers[72] suggested that IVR, IC, ISC, and solvent reorganization may be occurring concurrently or on similar time scales. Their time-resolved results for a MLCT transition in a different compound are similar to our results for the platinum acetylide complex **1** presented here. Our frequency domain approach using resonance Raman and fluorescence emission complements the femtosecond time-resolved experiments like transient absorption and it would be quite useful to have both results for comparison to calculated results from various theoretical models to help develop an improved understanding of the ultrafast molecular dynamics (both solvent and solute) of the photoinduced electron transfer process in transition metal complexes. Toward this goal we are presently undertaking a reinvestigation of the $[Ru(bpy)_3]^{2+}$ complex in acetonitrile solvent using resonance Raman and fluorescence spectroscopy for comparison to the femtosecond time-resolved results of McCusker and co-workers.[72] The results of this study will be reported in the future.

If it is fairly common for very fast dynamical processes (such as ISC) to take place from unequilibrated (i.e., unrelaxed) excited states, then this raises the possibility of using more of the stored energy of the absorptive state to accomplish photon induced

**TABLE 6: Comparison of Experimental and Calculated Resonance Raman Intensities of $[Pt_2(\mu\text{-dppm})_2(\mu\text{-PhC}{\equiv}C)(PhC{\equiv}C)_2]ClO_4$ (2) in Acetonitrile Solution**

| | | intensity | | | | | | | |
|---|---|---|---|---|---|---|---|---|---|
| | Raman | 368.9 nm | | 397.0 nm | | 416.0 nm | | 435.7 nm | |
| peak | shift[a] ($cm^{-1}$) | expt[b] | calc | expt[b] | calc | expt[b] | calc | expt[b] | calc |
| F | 179 | * | 9 | 17 | 17 | 8 | 22 | 22 | 27 |
| F | 216 | * | 10 | 19 | 19 | 14 | 24 | 12 | 29 |
| F | 261 | * | 55 | 100 | 100 | 39 | 128 | 26 | 152 |
| F | 382 | * | 81 | 140 | 140 | 85 | 174 | 87 | 202 |
| F | 421 | * | 15 | 26 | 26 | 23 | 32 | 20 | 37 |
| F | 452 | * | 37 | 62 | 62 | 27 | 76 | 38 | 87 |
| F | 529 | 97 | 64 | 103 | 103 | 55 | 125 | 44 | 140 |
| F | 552 | 24 | 13 | 23 | 23 | 17 | 28 | 6 | 3 |
| F | 568 | | 11 | 18 | 18 | 7 | 22 | 23 | 24 |
| F | 799 | 36 | 43 | 61 | 61 | 45 | 70 | 49 | 75 |
| F | 967 | 20 | 11 | 14 | 14 | | 15 | | 16 |
| F | 994 | 36 | 16 | 21 | 21 | 33 | 23 | 27 | 24 |
| F | 1095 | 7 | 9 | 11 | 11 | | 12 | | 12 |
| F | 1147 | 13 | 4 | 5 | 5 | | 5 | | 5 |
| F | 1170 | 37 | 25 | 30 | 30 | 42 | 32 | 42 | 33 |
| F | 1213 | 39 | 18 | 21 | 21 | 15 | 22 | 10 | 23 |
| F | 1481 | 8 | 7 | 7 | 7 | 7 | 7 | 6 | 7 |
| F | 1529 | 8 | 7 | 7 | 7 | 7 | 7 | 6 | 7 |
| F | 1589 | 100 | 100 | 100 | 100 | 100 | 100 | 100 | 100 |
| absol Raman c.s. of 1589 $cm^{-1}$ peak ($Å^2$/molecule) | | | | | | | | | |
| expt | | $[1.5 \times 10^{-9}]$ | | $[3.6 \times 10^{-9}]$ | | $[3.3 \times 10^{-9}]$ | | $[1.9 \times 10^{-9}]$ | |
| calc | | $(4.9 \times 10^{-9})$ | | $(3.7 \times 10^{-9})$ | | $(1.7 \times 10^{-9})$ | | $(4.7 \times 10^{-9})$ | |
| F | 1806 | 44 | 49 | 45 | 45 | 41 | 44 | 16 | 44 |
| F | 1996 | 56 | 62 | 53 | 53 | 65 | 51 | 75 | 51 |
| F | 2027 | 124 | 199 | 167 | 167 | 111 | 161 | 153 | 160 |
| F | 2062 | 116 | 261 | 217 | 217 | 140 | 208 | 81 | 207 |
| F | 2125 | 205 | 185 | 151 | 151 | 64 | 144 | 68 | 144 |
| absol Raman c.s. of 2125 $cm^{-1}$ peak ($Å^2$/molecule) | | | | | | | | | |
| expt | | $[3.1 \times 10^{-9}]$ | | $[5.5 \times 10^{-9}]$ | | $[2.1 \times 10^{-9}]$ | | $[1.3 \times 10^{-9}]$ | |
| calc | | $(9.1 \times 10^{-9})$ | | $(5.6 \times 10^{-9})$ | | $(2.4 \times 10^{-9})$ | | $(6.7 \times 10^{-10})$ | |

[a] Estimated uncertainties are about 4 $cm^{-1}$ for the Raman shifts. [b] Relative intensities are based on integrated areas of the peaks. Estimated uncertainties are about 10% for intensities 50 and higher, 15% for intensities between 15 and 50, and 30% for intensities lower than 15.

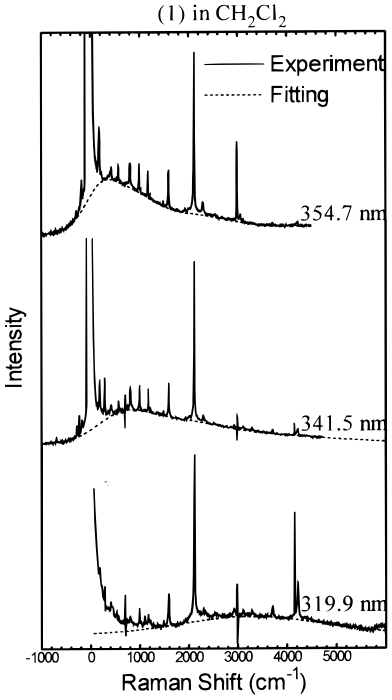


**Figure 6.** Expanded view of the fluorescence background found below the resonance Raman spectra of **1** for 319.9, 341.5, and 354.7 nm excitation wavelengths. The dashed curves estimate the shape of the fluorescence observed.

reactions. By carefully tailoring the molecular system one may be able to achieve much better yields of the desired photochemical reaction since less energy would be wasted through intramolecular energy distribution. It is interesting to note that both complex **1** (and possibly **2**) and the $[Ru(bpy)_3]^{2+}$ complex appear to have ultrafast ISC from unequilibrated states in the initially formed excited electronic state. This suggests it would be very worthwhile to explore the initial excited state dynamics of many different types of transition metal complexes which may be considered for building blocks in molecular photochemical devices.

We should note some caveats about our present study of the platinum acetylides **1** and **2**. The partially overlapping transitions of the absorption bands make it difficult to extract accurate quantitative information about the MLCT transition of **1** and the MMLCT transition of **2**. The resonance Raman intensity analyses presented here are meant to obtain semiquantitative information (or estimates) about the dominant transition contributing to the MLCT absorption of **1** and the dominant transition contributing to the MMLCT absorption of **2**. The parameters of Tables 3 and 5 (used in the single electronic state model to simulate the resonance Raman intensities and absorption spectra) should be regarded as initial estimates of characterizing the MLCT transition of **1** and the MMLCT transition of **2**. These initial estimates could be significantly improved with a more complete excitation profile of the intensities and simulations using a multiple electronic state model. We are currently investigating substituent effects on the initial excited state Franck−Condon region dynamics of several platinum acetylide complexes such as $Pt(PEt_3)_2(C{\equiv}CH)_2$ which have much better resolved absorption bands. This will help minimize contributions to the resonance Raman intensities of the MLCT

absorption from other electronic transitions and likely allow us to extract more reliable quantitative information about the MLCT transitions of these platinum acetylide compounds. This work will subsequently be reported.

**Acknowledgment.** This work was supported by grants from the Committee on Research and Conference Grants (CRCG), the Research Grants Council (RGC) of Hong Kong, the Hung Hing Ying Physical Sciences Research Fund, and the Large Items of Equipment Allocation 1993−94 from the University of Hong Kong. The authors acknowledge Prof. A. B. Myers for a copy of the FORTRAN code used to carry out the time-dependent wavepacket calculations of the absolute resonance Raman intensities and absorption spectrum.

## References and Notes

(1) Sacksteder, L.-A.; Baralt, E.; DeGraff, B. A.; Lukehart, C. M.; Demas, J. N. *Inorg. Chem.* **1991**, *30*, 2468−2476.
(2) Baralt, E.; Lukehart, C. M. *Inorg. Chem.* **1991**, *30*, 319−320.
(3) Stoner, T. C.; Geib, S. J.; Hopkin, M. D. *J. Am. Chem. Soc.* **1992**, *114*, 4201−4204.
(4) Manna, J.; Geib, S. J.; Hopkin, M. D. *J. Am. Chem. Soc.* **1992**, *114*, 9199−9200.
(5) Yip, H.-K.; Lin, H.-M.; Wang, Y.; Che, C. M. *J. Chem. Soc., Dalton Trans.* **1993**, 2939−2944.
(6) Yam, V. W. W.; Chan, L.-P.; Lai, T.-F. *Organometallics* **1993**, *12*, 2197−2202.
(7) Masai, H.; Sonogashi, K.; Hagihara, N. *Bull. Chem. Soc. Jpn.* **1971**, *44*, 2226.
(8) Yam, V. W. W.; Chan, L. P.; Lai, T. F. *J. Chem. Soc., Dalton Trans.* **1993**, 2075−2077.
(9) Yam, V. W. W.; Fung, W. K. M.; Cheung, K. K. *Angew. Chem., Int. Ed. Engl.* **1996**, *35*, 1100−1102.
(10) Yam, V. W. W.; Choi, S. W. K.; Cheung, K. K. *Organometallics* **1996**, *15*, 1734−1739.
(11) Yam, V. W. W.; Choi, S. W. K. *J. Chem. Soc., Dalton Trans.* **1996**, 4227−4232.
(12) Marcus, R. A. *Annu. Rev. Phys. Chem.* **1964**, *15*, 155−196.
(13) Siders, P.; Marcus, R. A. *J. Am. Chem. Soc.* **1981**, *103*, 741−747.
(14) Siders, P.; Marcus, R. A. *J. Am. Chem. Soc.* **1981**, *103*, 748−752.
(15) Jortner, J. *J. Chem. Phys.* **1976**, *64*, 4860−4867.
(16) Buhks, E.; Bixon, M.; Jortner, J.; Navon, G. *J. Phys. Chem.* **1981**, *85*, 3759−3762.
(17) Van Duyne, R. P.; Fischer, S. F. *Chem. Phys.* **1974**, *5*, 183−197.
(18) Myers, A. B. *Chem. Phys.* **1994**, *180*, 215−230.
(19) Clark, R. J. H.; Stewart, B. *J. Am. Chem. Soc.* **1981**, *103*, 6593−6599.
(20) Clark, R. J. H.; Dines, T. J.; Wolf, M. L. *J. Chem. Soc., Faraday Trans. 2* **1982**, *78*, 679−688.
(21) Clark, R. J. H.; Dines, T. J.; Proud, G. P. *J. Chem. Soc., Dalton Trans.* **1983**, 2019−2024.
(22) Clark, R. J. H.; Dines, T. J.; Doherty, J. M. *Inorg. Chem.* **1985**, *24*, 2088−2091.
(23) Clark, R. J. H.; Hempleman, A. J.; Dawes, H. M.; Hursthouse, M. B.; Flint, C. D. *J. Chem. Soc., Dalton Trans.* **1985**, 1775−1780.
(24) Yoo, C. S.; Zink, J. I. *Inorg. Chem.* **1983**, *22*, 2474−2476.
(25) Tutt, L.; Zink, J. I. *J. Am. Chem. Soc.* **1986**, *108*, 5830−5836.
(26) Hollingsworth, G.; Shin, K. S. K.; Zink, J. I. *Inorg. Chem.* **1990**, *29*, 2501−2506.
(27) Larson, L. J.; Zink, J. I. *Inorg. Chem.* **1989**, *28*, 3519−3523.
(28) Hanna, S. D.; Zink, J. I. *Inorg. Chem.* **1996**, *35*, 297−302.
(29) Shin, K. S.; Clark, R. J. H.; Zink, J. I. *J. Am. Chem. Soc.* **1989**, *111*, 4244−4250.
(30) Shin, K. S. K.; Clark, R. J. H.; Zink, J. I. *J. Am. Chem. Soc.* **1990**, *112*, 3754−3759.
(31) Doorn, S. K.; Hupp, J. T. *J. Am. Chem. Soc.* **1989**, *111*, 1142−1144.
(32) Doorn, S. K.; Hupp, J. T. *J. Am. Chem. Soc.* **1989**, *111*, 4704−4712.
(33) Doorn, S. K.; Hupp, J. T.; Porterfield, D. R.; Campion, A.; Chase, D. B. *J. Am. Chem. Soc.* **1990**, *112*, 4999−5002.
(34) Blackbourn, R. L.; Johnson, C. S.; Hupp, J. T.; Bryant, M. A.; Sobocinski, R. L.; Pemberton, J. E. *J. Phys. Chem.* **1991**, *95*, 10535−10537.
(35) Wright, P. G.; Stein, P.; Burke, J. M.; Spiro, T. G. *J. Am. Chem. Soc.* **1979**, *101*, 3531−3535.
(36) Yang, Y. Y.; Zink, J. I. *J. Am. Chem. Soc.* **1984**, *106*, 1500−1501.
(37) Wootton, J. L.; Zink, J. I. *J. Phys. Chem.* **1995**, *99*, 7251−7257.
(38) Pedron, D.; Speghini, A.; Mulloni, V.; Bozio, R. *J. Chem. Phys.* **1995**, *103*, 2795−2809.
(39) Fraga, E.; Webb, M. A.; Loppnow, G. R. *J. Phys. Chem.* **1996**, *100*, 3278−3287.
(40) Britt, B. M.; Lueck, H. B.; McHale, J. L. *Chem. Phys. Lett.* **1992**, *190*, 528−532.
(41) Britt, B. M.; McHale, J. L.; Friedrich, D. M. *J. Phys. Chem.* **1995**, *99*, 6347−6355.
(42) Markel, F.; Ferris, N. S.; Gould, I. R.; Myers, A. B. *J. Am. Chem. Soc.* **1992**, *114*, 6208−6219.
(43) Kulinowski, K.; Gould, I. R.; Myers, A. B. *J. Phys. Chem.* **1995**, *99*, 9017−9026.
(44) Kulinowski, K.; Gould, I. R.; Ferris, N. S.; Myers, A. B. *J. Phys. Chem.* **1995**, *99*, 17715−17723.
(45) Phillips, D. L.; Gould, I. R.; Verhoeven, J. W.; Tittlebach-Helmrich, D.; Myers, A. B. *Chem. Phys. Lett.* **1996**, *258*, 87−93.
(46) Langrick, C. R.; McEwan, D. M.; Pringle, P. G.; Shaw, B. L. *J. Chem. Soc., Dalton Trans.* **1983**, 2487−2493.
(47) Kwok, W. M.; Phillips, D. L. *Chem. Phys. Lett.* **1995**, *235*, 260−267.
(48) Man, S.-Q.; Kwok, W. M.; Phillips, D. L. *J. Phys. Chem.* **1995**, *99*, 15705−15708.
(49) Kwok, W. M.; Phillips, D. L. *J. Chem. Phys.* **1996**, *104*, 2529−2540.
(50) Kwok, W. M.; Phillips, D. L. *J. Chem. Phys.* **1996**, *104*, 9816−9832.
(51) Man, S.-Q.; Kwok, W. M.; Johnson, A. E.; Phillips, D. L. *J. Chem. Phys.* **1996**, *105*, 5842−5857.
(52) Kwok, W. M.; Phillips, D. L.; Yeung, P. K.-Y.; Yam, V. W. W. *Chem. Phys. Lett.* **1996**, *262*, 699−708.
(53) Myers, A. B.; Li, B.; Ci, X. *J. Chem. Phys.* **1989**, *89*, 1876−1886.
(54) Trulson, M. O.; Mathies, R. A. *J. Chem. Phys.* **1986**, *84*, 2068−2074.
(55) Dudik, J. M.; Johnson, C. R.; Asher, S. A. *J. Chem. Phys.* **1985**, *82*, 1732−1740.
(56) Trulson, M. O.; Dollinger, G. D.; Mathies, R. A. *J. Chem. Phys.* **1989**, *90*, 4274−4281.
(57) Heller, E. J. *J. Chem. Phys.* **1975**, *62*, 1544−1555.
(58) Lee, S. Y.; Heller, E. J. *J. Chem. Phys.* **1979**, *71*, 4777−4788.
(59) Heller, E. J.; Sundberg, R. L.; Tannor, D. J. *J. Phys. Chem.* **1982**, *86*, 1822−1833.
(60) Myers, A. B.; Mathies, R. A.; Tannor, D. J.; Heller, E. J. *J. Chem. Phys.* **1982**, *77*, 3857−3866.
(61) Tutt, L.; Tannor, D.; Heller, E. J.; Zink, J. I. *Inorg. Chem.* **1982**, *21*, 3858−3859.
(62) Tutt, L.; Tannor, D.; Schindler, J.; Heller, E. J.; Zink, J. I. *J. Phys. Chem.* **1983**, *87*, 3017−3019.
(63) Myers, A. B.; Mathies, R. A. *Biological Applications of Raman Spectroscopy*; Wiley: New York, 1987; pp 1−58.
(64) Clark, R. J. H.; Dines, T. J. *Agnew. Chem., Int. Ed. Engl.* **1986**, *98*, 131−160.
(65) Zink, J. I.; Shin, K. S. K. *Adv. Photochem.* **1991**, *16*, 119−214.
(66) Myers, A. B. *Laser Techniques in Chemistry*; Wiley: New York, 1995; pp 325−384.
(67) Li, B.; Johnson, A. E.; Mukamel, S.; Myers, A. B. *J. Am. Chem. Soc.* **1994**, *116*, 11039−11047.
(68) Yan, Y. J.; Mukamel, S. *J. Chem. Phys.* **1987**, *86*, 6085−6107.
(69) Perrealt, D.; Drouin, M.; Michel, A.; Miskowski, V. M.; Schaefer, W. P.; Harvey, P. D. *Inorg. Chem.* **1992**, *31*, 695−702.
(70) Nagasawa, Y.; Yartsev, A. P.; Tominaga, K.; Bisht, P. B.; Johnson, A. E.; Yoshihara, K. *J. Phys. Chem.* **1995**, *99*, 653−662.
(71) Barbara, P. F.; Jarzeba, W. *Adv. Photochem.* **1990**, *15*, 1−68.
(72) Damrauer, N. H.; Cerullo, G.; Yeh, A.; Boussie, T. R.; Shank, C. V.; McCusker, J. R. *Science* **1997**, *275*, 54−57.
(73) Maroncelli, M. *J. Chem. Phys.* **1991**, *94*, 2084−2103.
(74) Rosenthal, S. J.; Xie, X.; Du, M.; Fleming, G. *J. Chem. Phys.* **1991**, *95*, 4715−4718.
(75) McMorrow, D.; Lotshaw, W. T. *J. Chem. Phys.* **1990**, *93*, 2160−2162.
(76) Kumar, P. V.; Maroncelli, M. *J. Chem. Phys.* **1995**, *103*, 3038−3060.